Histamine Effects on Endothelial Cell Fibronectin Interaction Studied by Atomic Force Microscopy

Andreea Trache,* Jerome P. Trzeciakowski,† Lesley Gardiner,* Zhe Sun,* Mariappan Muthuchamy,* Mingzhang Guo,‡ Sarah Y. Yuan,‡ and Gerald A. Meininger*

*Department of Medical Physiology, †Department of Pharmacology and Toxicology, and ‡Department of Surgery, Cardiovascular Research Institute, Texas A&M University System, College Station, Texas 77843-1114

ABSTRACT Atomic force microscopy was used to investigate the cellular response to histamine, one of the major inflammatory mediators that cause endothelial hyperpermeability and vascular leakage. AFM probes were labeled with fibronectin and used to measure binding strength between $\alpha5\beta1$ integrin and fibronectin by quantifying the force required to break single fibronectin-integrin bonds. The cytoskeletal changes, binding probability, and adhesion force before and after histamine treatment on endothelial cells were monitored. Cell topography measurements indicated that histamine induces cell shrinkage. Local cell stiffness and binding probability increased twofold after histamine treatment. The force necessary to rupture single $\alpha5\beta1$-fibronectin bond increased from 34.0 $\pm$ 0.5 pN in control cells to 39 $\pm$ 1 pN after histamine treatment. Experiments were also conducted to confirm the specificity of the $\alpha5\beta1$-fibronectin interaction. In the presence of soluble GRGDdSP the probability of adhesion events decreased >50% whereas the adhesion force between $\alpha5\beta1$ and fibronectin remained unchanged. These data indicate that extracellular matrix-integrin interactions play an important role in the endothelial cell response to changes of external chemical mediators. These changes can be recorded as direct measurements on live endothelial cells by using atomic force microscopy.

INTRODUCTION

The vascular endothelium forms a semipermeable membrane that controls blood-tissue exchange. The integrity of this barrier is maintained by equilibrium between the contractile/retractile force generated by the endothelial cytoskeleton and the adhesive forces produced at cell-cell junctional connections and cell-matrix focal contacts. Dynamic interactions occur among these structural elements in response to external chemical or physical stimuli, resulting in opening of the paracellular pathways for blood components to move across the vessel wall (1,2). This process, namely, endothelial hyperpermeability, is a major factor underlying the development of vascular leakage and tissue edema during inflammation and injury. In view of the importance of integrins in maintaining the interactions between cell and the extracellular matrix (ECM) it was hypothesized that changes in integrin function would be an important component of the responses to an inflammatory mediator.

Integrins are heterodimeric cell surface receptors composed of two noncovalently associated transmembrane subunits-α and -β, which connect adhesive proteins in the ECM to the cytoskeleton, and are also involved in intracellular signal transduction. There are 17 different α-subunits and eight different β-subunits identified at present, which associate to form >20 different receptors recognizing one or more extracellular ligands (3,4). Integrins are involved in force transmission, due to their connection with the cell matrix and cytoskeleton, and signal transduction due to their association with focal contacts. Fibronectin is one of the ECM proteins that promotes adhesion of endothelial cells to the basal membrane by binding to integrin receptors through functional specialized domains such as arginine-glycine-aspartate (RGD sequence) (5). Among the multitude of integrin receptors identified on the surface of vascular endothelial cells, integrin $\alpha5\beta1$ appears to be critical in the establishment of the endothelial monolayer (6). Also, it has been identified as the major fibronectin receptor recognizing the RGD sequence in fibronectin type III. Endothelial cell detachment from fibronectin has been observed as a result of cell treatment with soluble synthetic peptides that compete with ECM proteins at integrin binding sites. RGD-containing peptides are also reported to produce significant increases in permeability of isolated venules (6). These studies suggest an important role for fibronectin and the $\alpha5\beta1$ integrin.

Histamine is a hyperpermeability mediator involved in the inflammatory response. Conventionally, this type of mediator is known to cause vascular barrier dysfunction by inducing endothelial cell contraction and intercellular gap formation (5). Accumulating experimental evidence indicates that inflammatory mediators may affect the barrier function by altering endothelial cell-matrix adhesions (7–9). Within this context, the intracellular signaling response to inflammatory mediators could induce an inside-out reduction in cell-matrix adhesion, weakening the attachment or even causing detachment of the endothelial lining from its basement membrane. Conversely, the inflammatory signals may activate cell-matrix interactions, resulting in focal contacts assembly and redistribution. This could lead to a strengthened

Submitted December 1, 2004, and accepted for publication July 7, 2005.

Address reprint requests to Gerald A. Meininger, PhD, Texas A&M University, Health Science Center, Dept. of Medical Physiology, 336 Joe H. Reynolds Medical Bldg., College Station, TX 77843-1114. Tel.: 979-845-7491; Fax: 979-862-4638; E-mail: gam@tamu.edu.

0006-3495/05/10/2888/11 $2.00

doi: 10.1529/biophysj.104.057026

cell-matrix binding and provides an anchorage support for cells to adhere and form intercellular gaps (10). At this time it is unclear how the processes of intercellular gap formation and cell-ECM binding to the basement membrane cooperate to increase permeability. A goal of this study is to investigate the ability of histamine to alter integrin function with respect to fibronectin.

This study reports on the interaction between $\alpha5\beta1$ and fibronectin in endothelial cells in the absence and presence of histamine using atomic force microscopy. We hypothesized that histamine would induce detectable morphological changes at cellular level and would alter activity and binding force between fibronectin and $\alpha5\beta1$ integrin present on the endothelial cell surface.

MATERIALS AND METHODS

Cell isolation and cell culture

Porcine aortic endothelial cells (EC) or bovine coronary venular endothelial cells were isolated and maintained as described previously (11,12). The cells were trypsinized and then centrifuged to form a pellet. The cell pellet was dispersed in cell-culture media and the cells were grown on gelatin-coated dishes in a humidified incubator (Heraeus Instruments, Newtown, CT) in 5% CO_2 at 37°C in Dulbecco's modified eagle medium (DMEM/F-12) supplemented with 20% (for aortic EC) or 10% (for coronary venular EC) fetal bovine serum and 10 mM HEPES (Sigma, St. Louis, MO), 2 mM L-Glutamine, 1 mM sodium pyruvate, 25 units/ml heparin, and 100 units/ml penicillin, 100 μg/ml streptomycin, and 0.25 μg/ml amphotricin B (PSA). After 48 h the cells were placed in serum-free media supplemented with 1% bovine serum albumin (Sigma) for 16–20 h. All experiments were performed using cells in serum-free cell culture media, at room temperature. Unless otherwise specified, all reagents were purchased from GibcoBRL (Carlsbad, CA).

Instrumentation

The atomic force microscope (AFM) is an important tool (13) for studying biological samples due to its ability to image surfaces in liquids. The principle of operation of the AFM consists of physically interacting a cantilever tip with the molecules on the cell surface. Adhesion forces between the tip and cell surface molecules are detected as cantilever deflections. Thus, the cantilever tip can be used to image live cells with atomic resolution (14–17), and to probe singular molecular events in living cells under physiological conditions (18–22). Currently, this is the only technique available to directly provide both structural and functional information at high resolution.

The experiments were performed using a Bioscope system from Digital Instruments (Santa Barbara, CA), which was mounted on top of a modified Axiovert 100 TV inverted optical microscope (Carl Zeiss, Jena, Germany). The Bioscope system is equipped with a Nanoscope IIIa controller and Nanoscope III 5.12 software. Also, special glass holders and protective silicon sleeves allow use of the instrument for measurements in liquid. The inverted microscope permits cell visualization using a Zeiss objective 32× air, N.A. = 0.4. The real-time images are displayed on the computer monitor using a video camera (Pulnix, model TM 34KC, Yokohama, Japan). All force data were processed with proprietary software NForceR (copyright pending).

AFM probe labeling

Experiments were performed with unsharpened silicon nitride cantilevers purchased from ThermoMicroscopes (Sunnyvale, CA). The triangular cantilever configuration was used, measuring 320 μm in length and 22 μm width with a pyramidal half-angle of 35° and a spring constant of 13 ± 1 pN/nm. The cantilever spring constant was measured by Asylum Research (Santa Barbara, CA) using the thermal noise method (23,24).

For adhesion force measurements the probes were coated (25) with 1 mg/ml fibronectin (FN). Polyethylene glycol ((PEG) Sigma) 10 mg/ml was used to cross-link fibronectin onto the probes at room temperature (26). After the tip was mounted on the glass holder and washed, it was incubated with PEG for 5 min, washed five times with deionized water, and then incubated for 1 min with fibronectin. The tip was then washed again five times with phosphate buffered saline and mounted on the AFM head. The coating was performed only at the very end of the cantilever. The spring constant was assumed to be unchanged after protein labeling.

Histamine treatment

For all experiments, histamine (Sigma) was used at 10 μM. For imaging experiments, histamine was added directly to the cell culture dish and cells were incubated for 30 min. For adhesion force measurements, the histamine-containing media were added to the cells 5 min before the start of the experiment.

Single-cell AFM imaging

To obtain images of single cells in culture, the AFM was operated under fluid in contact mode. In the scanning process, the instrument was set to apply a constant force on the cell. In each horizontal line scan, both height data (z axis) and the position of the probe (deflection data) were recorded in the Nanoscope software. The maximum scanned image size was 100 × 100 μm with a scan speed of ~40 μm/s. Image acquisition time was on the order of 20–25 min for one image. Single cell imaging experiments were repeated for six cells.

AFM adhesion force and elasticity measurements

For force measurements the AFM was operated in force mode. In this mode, measurements on the relative stiffness of the cell surface (approach curve) were acquired in combination with force adhesion measurements between the AFM tip and the cell surface (retraction curve) (Fig. 1 *a*). In force mode, the piezotransducer (PZT) was set to drive the cantilever to touch and retract over a predefined distance in the z axis. The z axis movement of the PZT and the deflection signal from the cantilever were recorded in a force curve. When the probe was extended toward the cell surface (*A*), a cell contact point was established (*B*) and thereafter the cell surface was indented. Because of the cell stiffness, further probe extension causes an opposing force of increasing magnitude to be generated along with increasing indentation in the cell membrane (*B–C*). The upward deflection of the cantilever as it bends in response to this force, results in an increasing deflection signal. The membrane indentation part of the force curve was analyzed using the Hertz model (27) to obtain the apparent values of the Young modulus of elasticity. When the probe was retracted from the sample (*C–D*), the force between probe and sample gradually decreased until the cantilever returned to the original position. At this point the deflection signal also returned to the original value. However, if adhesion occurred between the probe and sample surface, the adhesion force causes the cantilever to bend downward, and the deflection signal fell below the original value. When the adhesion was broken (*D*), the cantilever rapidly returned to the original position, and a deflection (unbinding or adhesion event) was recorded on the retraction force curve. The adhesion force was calculated by multiplying the deflection height associated with the unbinding event and the spring constant of the cantilever. The labeled probes were set to repeatedly touch and retract from the cell surface at 0.8 μm/s. All force measurements were acquired at positions midway between the nucleus and the edge of the cell for 30 min/cell and repeated for six cells. The time necessary to acquire one set of force curves (approach and retraction) was 2 s. Force measurements lying within

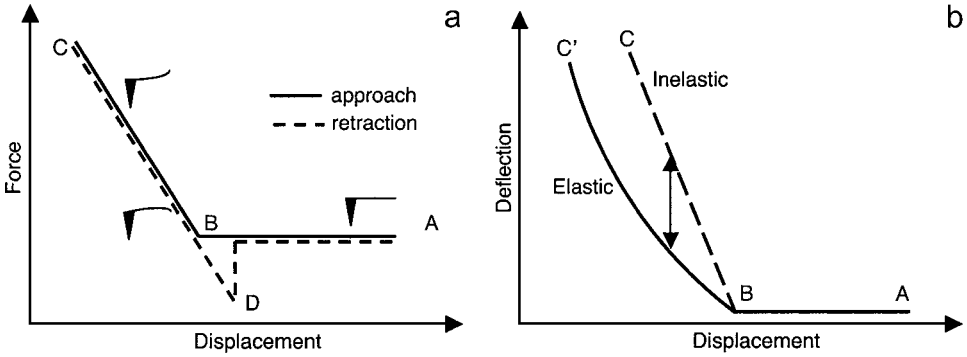

FIGURE 1 (*a*) Diagram of generic force curves (approach curve, *solid line*; retraction curve, *dashed line*). The *x* axis represents the PZT displacement and the *y* axis represents the force calculated as the product between the cantilever deflection and the spring constant of the cantilever. When the AFM tip approaches the sample (going from *right to left*) first there is no deflection (noncontact) regime (*A*). Moving the tip further toward the sample, there is a moment when the tip reaches the surface and establishes contact (*B*). Moving the tip further in the same direction causes deflection of the cantilever (contact regime). At a certain indentation (*C*), the tip begins to move away from the sample, causing the tip to bend upward, and finally detach from the sample (*D*) and loose contact (*A*). (*b*) Diagram of two combined approach force curves of elastic and inelastic material: the *x* axis represents the PZT displacement and *y* axis represents the deflection of the cantilever. For inelastic materials that are not deformable (elastic constant of the surface $\gg$ spring constant of cantilever) the amount of deflection of the tip in the contact regime (*B–C*) is equal to the amount of PZT movement (*dashed line*). If the sample is elastic and deformable, then the tip motion is larger than the deflection of the cantilever (*B–C′*). The difference between the tip motion and the cantilever deflection represents the tip indentation in the sample surface.

the noise region (<18 pN) were excluded from analysis (28,29). The data processing for force and stiffness measurements was performed using proprietary software NForceR (copyright pending) that detected and recorded all deflections associated with adhesion events in each of the experimental force curves.

As explained above, controlled movement of the AFM probe in the *z*-direction was used to apply various forces to the sample. On soft samples such as cells this resulted in an indentation of the cell, which is a measure of the local elastic properties of the cell. If the cell was rigid, then for each 1 nm of PZT movement in the negative *z*-direction, there would be 1 nm of probe deflection in the positive *z*-direction caused by bending of the cantilever. Because of the elastic properties of the cell membrane, however, only a portion of the PZT movement causes deflection of the probe; the remainder results in depression or indentation of the membrane. The difference between the actual plot of deflection versus displacement and the theoretical line expected for an inelastic solid gives a measure of the indentation (Fig. 1 *b*). The degree of bending or curvature of the displacement curve after cell surface contact describes the local elastic properties of the cell (e.g., the softer the cell the less the curve bends upward and away from the horizontal precontact part).

To calculate the elasticity of a sample quantitatively, a theoretical model was fitted to the portion of the approach curve between the initial point of cell contact and the point of maximal probe displacement. Hertz (27) was the first to report a simple analytical solution for the elastic deformation that takes place between two spheres in contact under load. Sneddon (30), using a modern mathematical approach in cylindrical coordinates, extended this model to a cone indenting a flat surface. His approach continues to be referred to as the Hertz model (31,32). The model was designed for the ideal case of a homogeneous, flat, and elastic sample, and was applied here in an approximate manner to derive the apparent modulus of elasticity of the cell at the point of indentation (33). This model gives a direct relationship between the loading force F and the indentation δ into the cell body:

$$F = \frac{2}{\pi}\frac{E}{(1-\nu^2)}\frac{\delta^2}{\tan\alpha} \text{ with } r_{\text{cone}} = \frac{2}{\pi}\frac{\delta}{\tan\alpha}, \qquad (1)$$

where E is the apparent Young's modulus of the cell at the point of indentation, α the half-opening angle of the indenting cone, and ν the Poisson ratio of the cell, assumed to be 0.5. In applying the Hertz model, the probe tip is considered a cone, and the cell membrane, though curved at cell scale, is considered as a flat surface. Given the small area of the probe tip in contact with the membrane, the initial curvature of the surface over this region was assumed insignificant. For analyzing experimental data, the *z*-displacement and the cantilever deflection d were expressed relative to an offset, taken as the point at which the probe tip first contacted the cell surface. If the point of contact (offset) is given by (z_0, d_0), then Eq. 1 becomes:

$$F = k\,d_{\text{m}} = \frac{2}{\pi}\frac{E}{(1-\nu^2)}\frac{(z_{\text{m}}-d_{\text{m}})^2}{\tan\alpha}, \qquad (2)$$

where $z_{\text{m}} = z - z_{\text{o}}$ indicates the relative probe displacement and $d_{\text{m}} = d - d_{\text{o}}$ the relative probe deflection. Note that the force F is estimated from the product of the relative probe deflection d_{m} and the cantilever spring constant k, and the quantity $(z_{\text{m}} - d_{\text{m}})$ denotes the difference between the relative probe displacement and relative probe deflection being a measure of the membrane indentation. Equation 2 can be rearranged to give:

$$d_{\text{m}} = \left(\frac{2}{\pi}\frac{E}{k(1-\nu^2)\tan\alpha}\right)(z_{\text{m}}-d_{\text{m}})^2. \qquad (3)$$

The apparent elastic modulus E can be calculated by fitting the relationship between relative probe displacement and indentation, knowing k, ν, and α. On average, similar results are obtained by using the initial portion of the retraction curve, up to and including the point corresponding to the offset that was determined from the approach curve.

$\alpha_5\beta_1$ Specificity

To test the specificity of the fibronectin-$\alpha_5\beta_1$ integrin interaction, force measurements were repeated in the presence of GRGDdSP (Bachem Biosciences, King of Prussia, PA), an $\alpha_5\beta_1$ specific ligand (6,34), or GRGESP (GibcoBRL, Carlsbad, CA), an inactive control. The concentration used in the experiments was 0.5 mM for both the active ligand as well as the inactive control peptide. The peptide-containing media were added to the cell culture dish, with an incubation time of 15 min at room temperature. Force measurements were acquired for 2 min per cell and repeated for 20 cells.

Statistical analysis

To test for significant changes in force or apparent elastic modulus over time, regression lines were fitted to each set of data and the slopes (trends) were compared statistically. Differences in adhesion counts were tested two ways. To evaluate adhesion counts globally between the control and histamine-treated cells, the number of adhesion events was tabulated for 30 min at 5-min intervals. Significance was tested with the Mantel-Haenszel χ^2 test with continuity correction (SPLUS v. 6.1, Insightful, Seattle, WA). Differences in

adhesions between the two treatment groups at each time were evaluated using Pearson's χ^2 test with Yates' continuity correction (SPLUS v. 6.1, Insightful). The force curves with no adhesion events were also counted. Note that the number of force curves analyzed and reported in this article is in thousands of curves per measurement. All results were presented as means $\pm$ SE. Significance was assumed at $p \leq 0.05$.

RESULTS

AFM imaging and endothelial cell topography

An AFM contact mode set of images of an isolated coronary venular EC before and after 30 min of treatment with histamine is presented in Fig. 2. The AFM deflection images are presented in the top row and the enhanced contrast height images are presented at the bottom. The deflection images are created by acquiring the cantilever deflection data on the z axis whereas the enhanced contrast images are obtained from height image data using a mask-based background correction technique to remove residual noise present at the time of the experiment. The deflection image emphasizes the main features of the cell: the round nucleus is surrounded by cytoplasm against the flat bottom of the dish. The main features of the cytoskeleton (actin filaments) are also visible as rod-like filaments around the cell edges. The enhanced contrast height image provided a more detailed image of the structure of the cytoskeleton with visible stress fibers in the cell cortex area and tight rod-like bundles around the peripheral edges.

Using the topographical cell data, direct measurements of cell coverage area, cell volume, and cell height of coronary venular ECs before and after histamine treatment were performed. The average values before and after histamine treatment are presented in Table 1. The percent change in cell coverage area, cell volume, and cell height was calculated as $\%\ change = ((treatment - control)\ /\ control) \times 100$. In nontreated cells over the 30-min period, there was a slight decrease ($<2\%$) in coverage area and a 5 and 4% increase in volume and height, respectively. These changes in control experiments were not statistically significant.

In contrast, histamine-treated cells displayed notable changes in cell shape with visible rearrangement of the cortical cytoskeleton after histamine treatment. In several parts of the cell, the peripheral rod-like actin bundles were disrupted and some small actin bundles look diminished or lost, but in the other parts the initial small actin bundles become more visible with formation of new strong rod-like structures (the actin network appeared to lose fine structure at the expense of enhancing the more robust structure; see *arrows* in Fig. 2). Also, important morphological changes took place. The average coverage area of the cells was reduced by 8% and volume decreased by 13% after the histamine treatment in comparison with control (Fig. 3). No significant change in cell height was observed probably because the nucleus plays the dominant role in determining the cell height. As a control to assess the ability of the AFM to detect cell volume

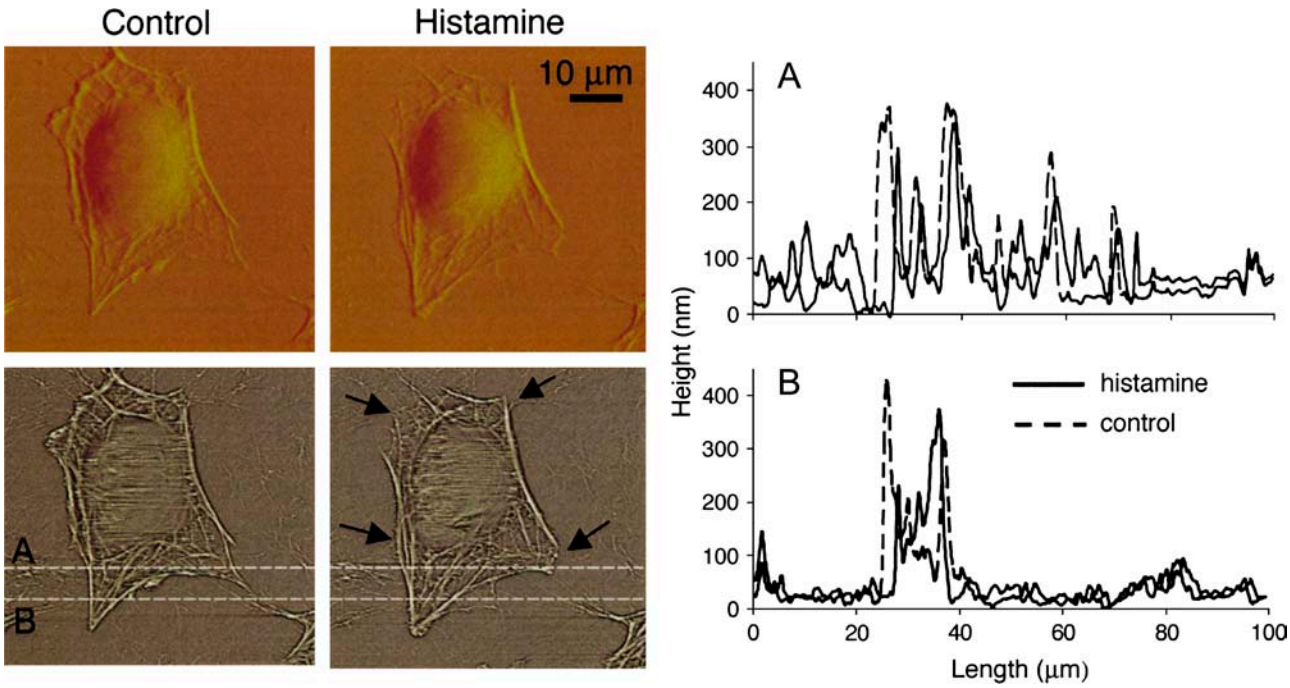

FIGURE 2 Contact mode images of an isolated coronary venular EC before and after histamine treatment. The upper row presents the deflection images and the lower row displays enhanced contrast height images. Rearrangement of cortical cytoskeleton and cell shrinkage after histamine treatment is visible (see *arrows*). Panels *A* and *B* in the graph represent two topographical profiles along the white dashed lines in the bottom panels. The *xy* scan rate used for imaging was 0.225 Hz for a scan size of 100×100 μm with a scan speed <40 μm/s. The deflection images were acquired directly in Nanoscope software and the enhanced contrast images were obtained by further processing of height data in Matlab software (MathWorks, Natick, MA). The bar represents 10 μm.

TABLE 1 Geometrical parameters

Coronary venular EC	Control		Histamine	
	Control	Vehicle	Control	Treatment
Cell coverage area (μm^2)	2069 ± 307	2039 ± 313	2362 ± 297	2154 ± 291
Volume (μm^3)	964 ± 145	1016 ± 100	1884 ± 166	1732 ± 223
Maximum height (nm)	2694 ± 243	2808 ± 115	2846 ± 266	2983 ± 366

changes, the coronary venular ECs were placed in a hypertonic solution (500 mOsm). A significant overall shrinkage of the cells was measured, with a decrease of 21% in cell volume and 10% decrease in cell coverage area, as well as gap formation between the cells. Likewise, when the coronary venular ECs were treated with 120 mM mannitol (Sigma) to induce cell swelling, a significant increase of 25% in cell volume was measured.

Fig. 4 shows an image of several coronary venular ECs in a subconfluent monolayer before (*a*) and after histamine treatment (*b*). Histamine induced visible gaps between the adjacent cells. The intercellular gaps began to form within minutes after the histamine treatment (<1 min). The process of gaps formation was completed within 20 min, at which point in time the post treatment images were acquired.

AFM force curve analysis of $\alpha 5\beta 1$ adhesion to fibronectin and histamine effect

To calculate the elasticity of a sample quantitatively, the theoretical model developed by Hertz was fitted to the portion of the approach curve between the initial point of cell contact and the point of maximal probe displacement. Fig. 5 shows changes in elastic modulus as a function of time and treatment. Histamine increased the stiffness of aortic ECs from an average value of the apparent elastic modulus of 8 ± 2 kPa ($n = 6$) for controls to an average value of 20 ± 5 kPa ($n = 6$) after treatment. This change represented more than a twofold increase. Based on statistical goodness of fit criteria ($r^2 > 0.9$), the data appeared well described by the Hertz model. The apparent elastic modulus represents the local elastic properties of the cell measured in an area midway between nucleus and the cell edge. The time-dependence curves for the apparent elastic modulus indicated that there was no significant change over time. In the case of coronary venular ECs the average value for the apparent elastic modulus was 10 ± 3 kPa ($n = 6$) for control experiments and was not significantly changed by histamine treatment 7.5 ± 2.5 kPa ($n = 6$).

The retraction trace of the force curves was used to characterize the specific interactions taking place between the functionalized probe and the surface of the cell. Analysis of the retraction trace of the force curves allowed determination of the number of adhesion events and the forces required to break each adhesion (i.e., integrin-fibronectin bonds). Fig. 6 shows a pair of force curves for an experiment with no adhesion events (*a*) and one with multiple adhesion events (*b*). When no adhesion events took place between the AFM probe and the cell (*a*) the force curves (approach and retraction) are almost superimposable with no remarkable events in the horizontal portion of the retraction curve. In panel *b*, however, three distinct adhesion events were discernable. Each adhesion that ruptures as a result of the retraction of the tip from the cell surface was characterized by a force, calculated by multiplying the height of the step in the deflection associated with the unbinding event and the spring constant of the cantilever.

Fig. 7 *a* presents the adhesion force measurements for an untreated (control) group of aortic ECs ($n = 6$). Adhesion forces were characterized by constructing histograms of the number of events detected at various forces. The midpoints in each histogram bar were then connected to approximate the envelope of the distribution. The distributions were analyzed further by fitting the entire envelope with multiple Gaussian density curves using a deconvolution algorithm. The analysis results in good agreement between the experimental points (*squares*) and the fitted envelope (*solid line*).

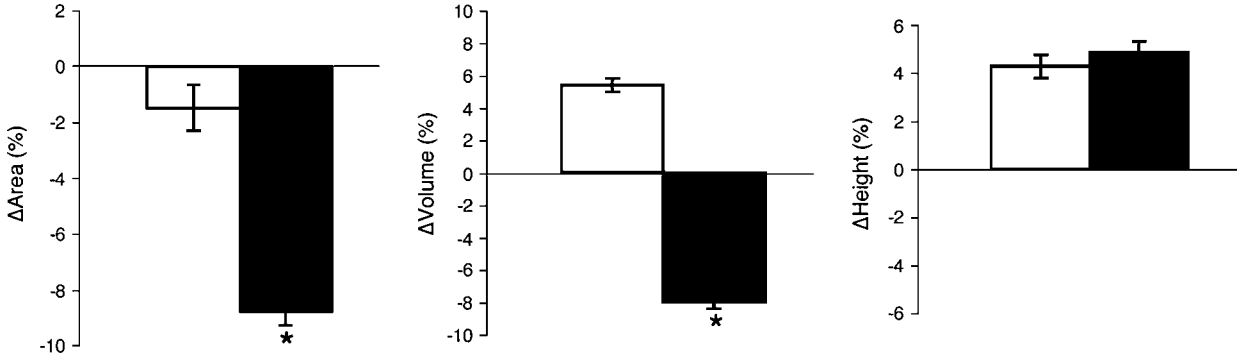

FIGURE 3 Relative change in geometrical parameters of the coronary venular EC for control experiment (*open bar*) and after histamine treatment (*solid bar*) (*$p < 0.05$).

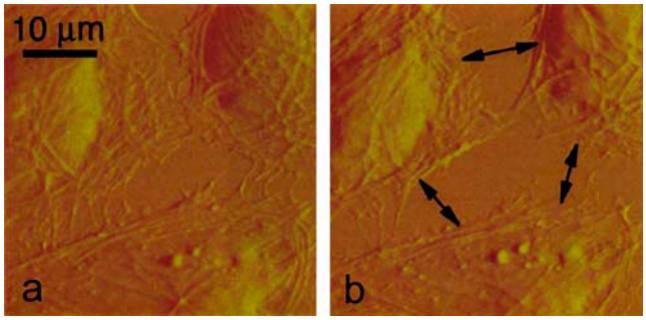

FIGURE 4 Image of a confluent coronary venular EC culture (*a*). Gaps were forming in the cell monolayer after histamine treatment (*b*). The bar represents 10 μm.

For control aortic ECs, three distinct Gaussian populations were apparent. The first dashed distribution (from *left to right*) represents the adhesion force of a single integrin-fibronectin bond having a value 34.0 $\pm$ 0.5 pN. This interpretation was suggested by the presence of a second and a third distribution with peaks equally spaced and at higher values 51 $\pm$ 1 and 67 $\pm$ 1 pN, respectively. It is possible that these peaks correspond to simultaneous rupture of two and three bonds, respectively. The vertical bar in the same figure presents the probability of adhesion events in the same experiment.

As mentioned before, all adhesion and nonadhesion events were counted and normalized to unity. The average probability of adhesion for the control experiment was 0.30 $\pm$ 0.05. Using this procedure, the control experimental data for aortic ECs already described were compared with those obtained after histamine treatment (Fig. 7 *b*). By comparing the force distributions before and after histamine treatment one can observe that the general shape of the resolved distributions are preserved. In the histamine-treated cells, peak forces occurred at 39 $\pm$ 1, 60 $\pm$ 2, and 81.5 $\pm$ 1.5 pN. Note that although the values of the peak force for all three Gaussian distributions are shifted toward higher values, they

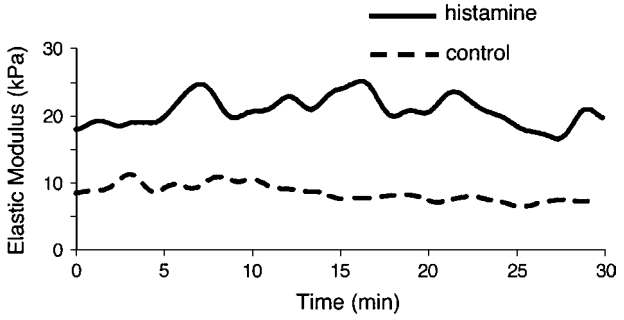

FIGURE 5 Elastic modulus for aortic EC. One can observe that there is no time dependence, but histamine treatment doubled the elastic modulus value (control, *dashed line*; histamine treatment, *solid line*). The apparent elastic modulus measurements were performed in a region midway between nucleus and the cell edge.

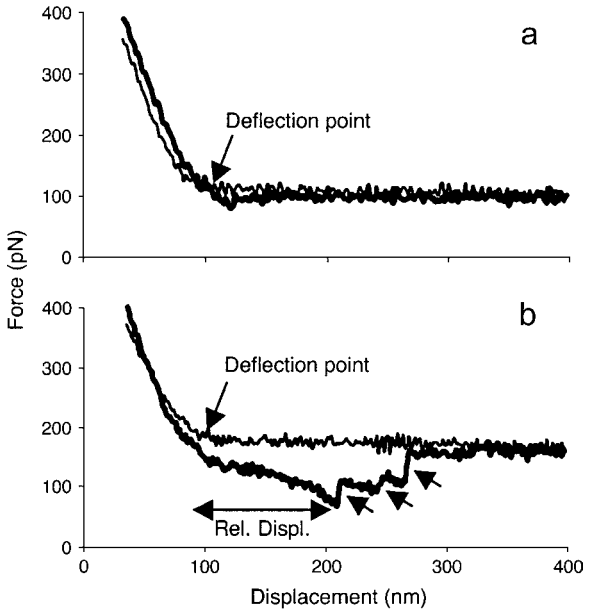

FIGURE 6 Approach (*thin line*) and retraction (*thick line*) force curves without adhesions (*a*) and with adhesions (*b*). The labeled probes were set to touch and retract from the cell surface at a speed of 0.8 μm/s. If specific adhesion events occurred between fibronectin and $\alpha5\beta1$ integrin during approach procedure, the retraction curve recorded the appearance of distinct bond ruptures indicated by arrows in panel *b*. Deflection point and relative displacement were calculated as explained in text.

are not shifted to the same degree. The largest peak increased by ~5 pN, the middle peak by ~10 pN, and the smallest peak increased by ~15 pN (Fig. 8).

After histamine treatment the probability of adhesion increased (Fig. 9). In addition, the number of adhesion events was higher at short relative displacements (~70 nm), and decreased to control level at long relative displacements (*a*). The relative displacement represents the distance between the deflection point and the location where an adhesion event occurs. In comparison, the number of adhesion events in control experiments was fairly constant over time but for histamine treatment it peaked at ~12 min after treatment (*b*). Analysis of the adhesion probability data (Fig. 10) indicated that the effect of histamine treatment was highly significant ($p = 0.001$) and reflects the fact that histamine caused a doubling of the number of adhesions compared with the control. Trend analysis of adhesion event probability indicates a slight decline in adhesions over time when both treatment groups were pooled ($p = 0.04$). However, within either individual group, no significant trend was detected (control $p = 0.32$; histamine $p = 0.07$) and the 95% confidence interval around the slopes of each of the regression lines included zero. The treatment over time interaction term was not significant ($p = 0.30$) confirming the visual impression that the trend lines for both treatment groups were essentially parallel. Given the lack of correlation between treatment and time, the Mantel-Haenszel test

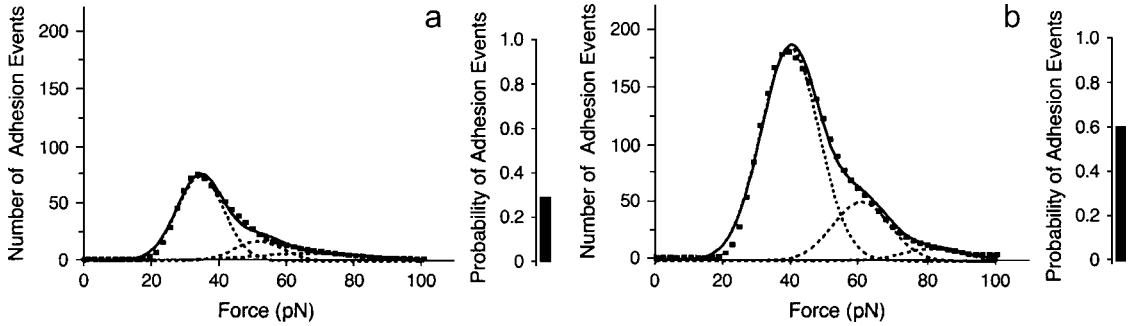

FIGURE 7 Analysis of force distributions of aortic EC before (*a*) and after (*b*) histamine treatment performed by simultaneous deconvolution of the experimental data (■) with Gaussian distributions to resolve the integrin-fibronectin binding forces. Although histamine treatment preserved the overall shape of the force distribution, it increased adhesion probability and shifted the entire force distribution toward higher force values. The histogram bar shows the probability of adhesion events.

was used to globally assess the association between treatment and number of adhesion events. The χ^2 value was 330, which at one degree of freedom gave $p = 0$. Separate tests comparing treatment at each of the five times gave χ^2 values ranging from 30 to 101, all of which were associated with $p = 0$.

The same analysis was performed for coronary venular ECs. The peak forces for control experiments occurred at 35 $\pm$ 1, 52.5 $\pm$ 3.7, and 72 $\pm$ 4 pN. There were no significant changes after the histamine treatment in peak forces or in adhesion events.

Selectivity of fibronectin for $\alpha5\beta1$ integrin

To confirm the specificity of the integrin-fibronectin interaction (6,34), experiments with soluble GRGDdSP (D-serine form of the GRGDSP) and GRGESP were conducted. Specificity results are summarized as distribution curves in Fig. 11. In the experiments with GRGDdSP the overall shape of the distribution was preserved, such that the position of the force peaks remained unchanged, but the binding probability was reduced >50% with respect to the experiments with GRGESP. Another observation that supports the specificity of interaction is that all Gaussian distributions were affected by the presence of soluble GRGDdSP in direct proportion with number of adhesions observed. The third peak was abolished.

DISCUSSION

The ability to image and study the surface of living cells under physiological conditions is one of the important advantages of using the AFM for biological investigations. The cell surface imaged by AFM provides three-dimensional quantitative information that allows analysis of endothelial cell mechanics and biochemistry at cellular and molecular levels. After histamine treatment of coronary venular ECs there were significant morphological changes and cortical cytoskeleton rearrangement. An 8% reduction in cell coverage area occurred along with a 13% decrease in cell volume. These changes were attributed to cell contraction and a resultant uniform shrinkage of the cell surface that is consistent with previous documentation of intercellular gap formation in histamine-treated endothelial monolayers (5,10,35).

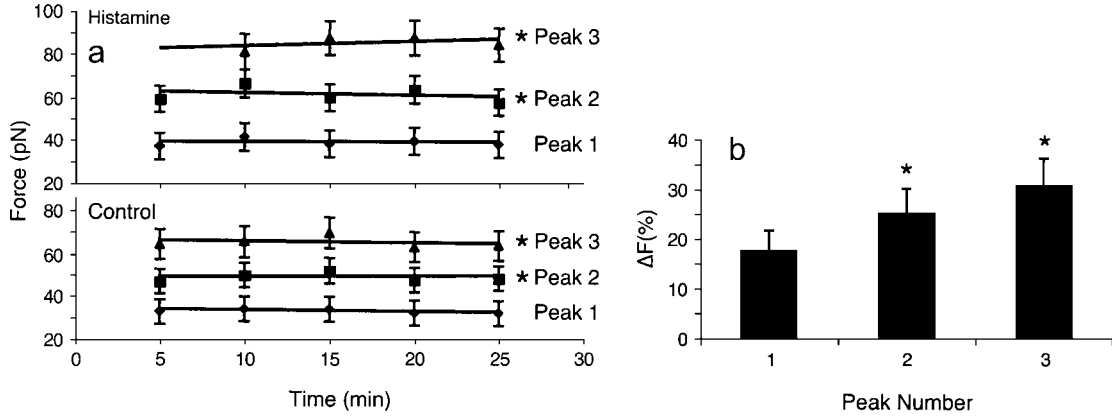

FIGURE 8 (*a*) Force versus time diagrams show that the force does not change in time, but increases as value after histamine treatment (*$p < 0.05$); (*b*) the relative change in adhesion force for each peak after histamine treatment.

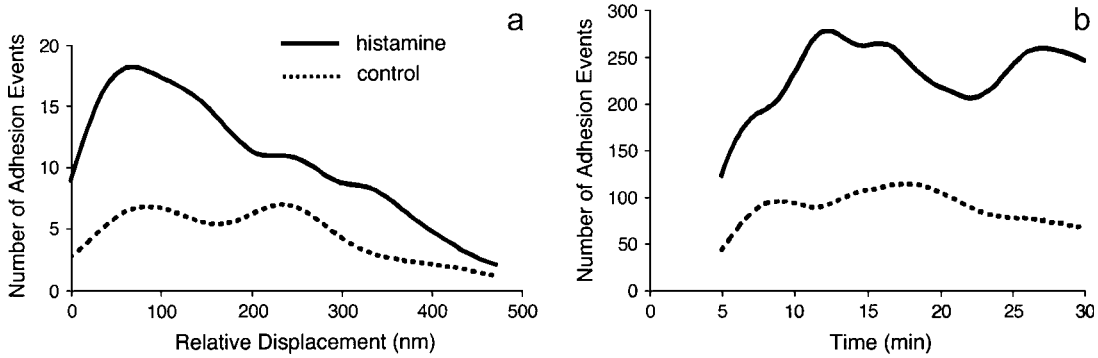

FIGURE 9 (*a*) After histamine treatment, not only the number of adhesion events increased, but the number was higher at short relative displacements followed by a decrease to the control level at long relative displacements. (*b*) For control experiments the number of adhesion events did not vary in time, but for histamine treatment it peaked at ~12 min and remained high for the duration of the experiment (*dotted line*, control; *solid line*, histamine treatment).

In addition to the morphological changes there was a visible rearrangement of the cortical cytoskeleton after histamine treatment. In several parts of the cell, the peripheral rod-like actin was disrupted and some small actin bundles look diminished or lost, but in the other parts the initial small actin bundles become more visible with formation of new strong rod-like structures. The change in the distribution of the actin network was not the result of AFM-induced damage to the cell surface, but resulted from a coordinated restructuring of the entire cytoskeleton network after histamine treatment (1,36). The cells were under continuous video observation during the imaging experiments and membrane dissection during AFM scanning was not observed.

For measuring the EC stiffness before and after histamine treatment the Hertz model was applied (27,30). To fit this model to the experimental force curves, the probe tip was approximated with a cone and the cell membrane assumed to be a flat surface. The Hertz model is designed to study a homogeneous, flat, and elastic sample. Even though the cells are heterogeneous in their elasticity and structural features (33), it was assumed that the Hertz model provides a good measure of the local apparent elastic modulus of the cell. This assumption is based on the consideration of the small area of the probe tip in contact with the cell membrane (tip radius ~50 nm), the thickness of the cell at the location where the measurement was performed (~1 μm) and the maximum measured indentation (<200 nm). Based on the Hertzian analysis, histamine treatment of aortic ECs caused the cells to become stiffer, such that the local apparent elastic modulus was twice the control value. The apparent elastic modulus values obtained in this study agree well with those reported in the literature. Weisenhorn et al. (32) reported values for the apparent elastic modulus of a living cell to be in the range of 13–15 kPa, Mathur et al. (37) reported for human umbilical vein endothelial cells a value for E between 1.4 and 6.8 kPa depending on the location of the measurement on the cell surface, Wojcikiewicz et al. (18) measured values for Young's modulus between 0.5 and 3 kPa for 3A9 cells, and Radmacher (38) reported values for apparent elastic modulus for living cells to be <20 kPa. All these values were obtained from AFM experiments.

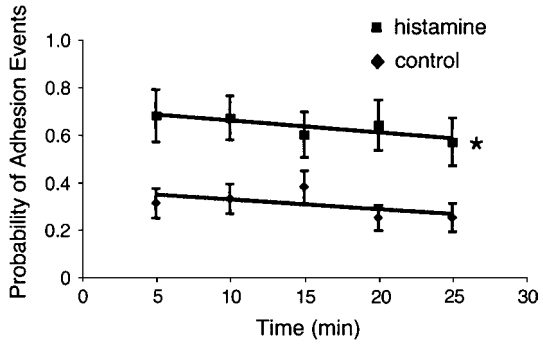

FIGURE 10 Probability of adhesion events increased twofold after histamine treatment (■) (*p = 0.001). Control experiment is presented with diamonds. Trend analysis indicated the same decline in adhesion events over time for both experiments (error bars represent ± SE).

The adhesion probability and the force necessary to break $\alpha5\beta1$-fibronectin bond were also increased by histamine treatment. To identify individual populations of adhesion forces, the overall force histogram obtained from adhesion measurements was deconvoluted using a method that resolves the experimental distribution into its components. In this way three distinct Gaussian distributions were separated under the main envelope of the overall histogram. The first resolved distribution was interpreted to represent the rupture of a single integrin-fibronectin bond, and subsequent distributions to represent ''simultaneous'' rupture of multiple adhesion bonds, with a time resolution of ~50 ms. Two arguments support the interpretation that the measurements represent ''simultaneous'' rupture of multiple bonds. First, the deconvoluted histograms of the force distributions appear as a series of discrete peaks and have their probabilities decreasing with the number of ruptured bonds. It is suggested that the measured force is actually the resultant force of the ''simultaneous'' rupture of multiple adhesion bonds. Second, this model is consistent with the force values obtained

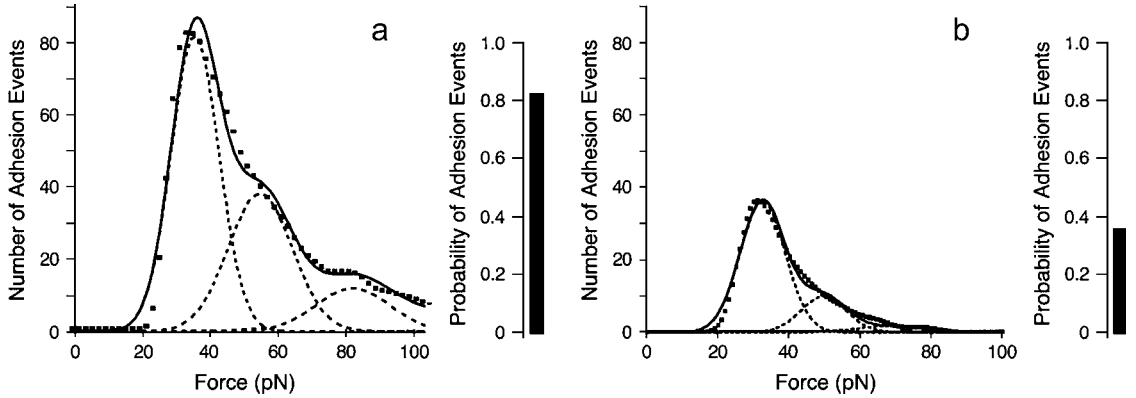

FIGURE 11 Analysis of force distributions for the GRGESP/GRGDdSP experiment. The GRGESP control force distributions (*a*) and the treatment GRGDdSP (*b*) are preserving the same overall shape, but GRGDdSP treatment recorded an important decrease in adhesion events. None of these peptides affected the magnitude of the adhesion force between fibronectin and $\alpha5\beta1$ integrin.

after histamine treatment where the peak forces are shifted at higher values in a progressive manner with an average value of ~5 pN for a single $\alpha5\beta1$-fibronectin bond.

The force values obtained through these experiments are in good agreement with those reported in the literature. Weisenhorn et al. (39) reported molecular forces on biological surfaces to be in the range of tens of piconewtons. Lehenkari and Horton (25) reported an AFM experiment for $\alpha5\beta1$ integrin-RGD peptide interaction on osteoblast a value of 32 ± 2 pN. Jiang et al. (40) measured adhesion forces in an optical trap experiment between fibronectin-coated beads and integrin on 3T3 fibroblasts in the range of 35–39 pN.

The possibility that the force measurements might represent processes other than rupture of $\alpha5\beta1$-fibronectin specific bonds was taken into consideration. Examples include: PEG or fibronectin detachment from the tip, PEG or fibronectin unfolding, integrin receptor pulling from the cell membrane, multiple binding conformations of FN on the probe tip, other FN receptors, or nonspecific binding. All of these possibilities could conceivably cause spread in force histograms. A possibility for not obtaining exact multiple integers for force peak values might be that the fibronectin could be adsorbed in multiple conformations (41) on the surface of the AFM tip. The method used for functionalizing the AFM tips does not provide any control of the possible fibronectin conformations on the tip. Also, based on the GRGDdSP data it appears that a major portion of adhesion events is specific. However, one cannot rule out completely the nonspecific binding to other receptors on the cell surface. It was concluded that the forces measured in this study were due primarily to the adhesion breakage between fibronectin and integrin based on the following arguments. Both, the absorption of PEG to the cantilever and PEG-fibronectin bond are much stronger than the measured adhesion forces (26,28). Also, protein unfolding requires a force of 11–15 pN, which is in the experimental noise and therefore is discarded due to a cutoff at 18 pN. It is unlikely that the receptors were being extracted from the membrane because the force needed to extract a transmembrane protein is ~160 pN, which is much larger than our measured forces (42). Also, it is unlikely that membrane rupture was being measured. Hundreds of cycles of binding and unbinding events per cell have been acquired with a single functionalized tip (43,44). If portions of the membrane were removed from the cell surface, then the contaminated tip would have a limited life span and cell death would occur. Neither of these events occurred in the studies reported here. Collectively, it was concluded that the adhesion forces measured in this study were primarily between the fibronectin functionalized tip and integrin receptors on the cell surface.

The increase in adhesion force between $\alpha5\beta1$ integrin and fibronectin in response to histamine may be part of the inflammatory process that reflects changes in cell-ECM interaction such as focal contacts assembly and redistribution. Moy et al. (10) estimated cell-ECM adhesion in confluent endothelial monolayers using electrical conductivity measurements and a theoretical model of current flow between adjacent cells and between the cells and underlying ECM. The parameter predicting cell-ECM adhesion fell below control through the first minute of histamine application. Cell-ECM adhesion returned to the normal level at 3 min, but continued to increase above the control level. Twenty minutes after exposure of the endothelial monolayer to histamine, cell-ECM adhesion was still above the control level. The AFM adhesion force measurements in our study were performed at 30 min and are consistent with the findings of Moy et al. (10). Thus, existing data support rapid changes in cell-ECM interactions in response to histamine.

Another possibility for increasing the adhesion after histamine treatment might be attributed to more integrins being able to bind the fibronectin on the apical cell surface because some of the cell-ECM interactions at the basal cell surface were severed (2), and more integrins are now free to diffuse to the apical cell surface. This is in good agreement with the

fact that the unbound integrins are freely diffusive in the membrane plane (45). A redistribution of integrins would hypothetically occur if focal contacts with the substrate were decreased in size or number (46,47).

The increase in cell stiffness that was recorded after histamine treatment may account for the increase in the adhesion force. In a study by Chen and Moy (42) it was shown that in an AFM experiment, after chemical fixation of the cell, the center of the first peak of the ligand-receptor adhesion force histogram was shifted in a small amount toward higher values, from 68 to 83 pN. This chemical fixation induces an increase in the loading rate by increasing cell stiffness that is similar to the cell stiffening after histamine treatment. The mechanism for the stiffness change after histamine treatment may be cytoskeletal in nature. Trepat et al. (48) used optical magnetic twisting cytometry to measure the cell complex elastic modulus calculated from the Fourier transform of the torque applied to magnetic beads (coated with RGD peptide) bound to membrane receptors. They showed that histamine induced reorganization of the actin cytoskeleton and formation of actin bundles, with a twofold increase in the complex elastic modulus of the cell.

Synthetic peptides that compete with ECM proteins for the integrin binding sites can be used to verify the specificity of $\alpha5\beta1$-fibronectin interaction. GRGDdSP is one such peptide that selectively inhibits $\alpha5\beta1$ integrin binding to fibronectin (6,34); $\alpha5\beta1$ is the major fibronectin receptor recognizing the RGD sequence on fibronectin type III. The RGD motif is displayed at the tip of a flexible loop projecting $\sim$10 Å from the FN III domain (49). In our experiments the binding probability between integrin and fibronectin was reduced $>$50% in the presence of soluble GRGDdSP peptide. It is suggested that the soluble specific ligand RGD competes with the FN-RGD sites on the AFM tip. It is important to note that the soluble RGD affects only the binding probability by reducing available integrin binding partners for the FN but does not affect the adhesion force.

Although our experiments were performed in cultured cells there are a few reports to indicate that AFM study of the intact EC layer of a vessel is possible. In these studies, vessels are splayed open to expose the EC layer to provide access for the AFM. Miyazaki and Hayashi (50) reported AFM measurements on living endothelial cells in fresh aorta segments under static strain from different areas. They found a high variability in the shape of force-indentation curves between cells, with the endothelial cells in the medial wall being stiffer than those in the lateral wall. Davies et al. (51) compared cell characteristics of the cultured cells with the vessel measurements, using confluent monolayers of aorta ECs in culture and aorta splayed vessels under flow. Using computational fluid dynamics combined with the AFM topographical measurements they found considerable variations in the distribution of forces on the individual cells and between neighboring cells. They concluded that the endothelial cell topography defines the detailed distribution of shear stresses at the single cell level. Further investigations using a splayed vessel with an intact EC layer for AFM studies could be pursued to assess the possibility of determining consistent parameters for stiffness and adhesion forces. This type of experiment might be useful for investigation of adhesion molecules on endothelial cells.

CONCLUSIONS

In this study we used AFM to image coronary venular EC before and after histamine treatment. Histamine affects morphological properties of the endothelial cells, producing cell shrinkage and endothelial gap formation in cultured ECs. By using the AFM to record direct measurements of the adhesion forces on the surface of the living endothelial cells, we have shown that the histamine treatment could change the binding probability but not the magnitude of adhesion force between $\alpha5\beta1$ and fibronectin. The force necessary to rupture single $\alpha5\beta1$-fibronectin bond increased from 34.0 ± 0.5 pN in control aortic ECs to 39 ± 1 pN after histamine treatment, whereas the adhesion probability increased twofold. Also, histamine treatment of aortic EC had a dramatic effect on local cell stiffness. The local apparent elastic modulus of the cell in a region midway between nucleus and cell edge was observed to increase twofold after histamine treatment. In summary, these data suggest that alteration in integrin binding probability and adhesion force may play a role in regulating the vascular endothelial barrier structure by altering cell-ECM interactions.

REFERENCES

1. Baldwin, A. L., and G. Thurston. 2001. Mechanics of endothelial cell architecture and vascular permeability. *Crit. Rev. Biomed. Eng.* 29: 247–278.
2. Yuan, S. Y. 2000. Signal transduction pathways in enhanced microvascular permeability. *Microcirculation.* 7:395–403.
3. Martinez-Lemus, L. A., X. Wu, E. Wilson, M. A. Hill, G. E. Davis, M. J. Davis, and G. A. Meininger. 2003. Integrins as unique receptors for vascular control. *J. Vasc. Res.* 40:211–233.
4. Humphries, M. J. 2000. Integrin structure. *Biochem. Soc. Trans.* 28: 311–339.
5. Lum, H., and A. B. Malik. 1996. Mechanisms of increased endothelial permeability. *Can. J. Physiol. Pharmacol.* 74:787–800.
6. Wu, M. H., E. Ustinova, and H. J. Granger. 2001. Integrin binding to fibronectin and vitronectin maintains the barrier function of isolated porcine coronary venules. *J. Physiol.* 532:785–791.
7. Wu, M. H., M. Guo, S. Y. Yuan, and H. J. Granger. 2003. Focal adhesion kinase contributes to VEGF-elicited microvascular hyperpermeability. *J. Physiol.* (*Lond.*). 552:691–699.
8. Guo, M., M. H. Wu, H. J. Granger, and S. Y. Yuan. 2005. Focal adhesion kinase in neutrophil-induced microvascular hyperpermeability. *Microcirculation.* 12:223–232.
9. Lampugnani, M. G., M. Resnati, E. Dejana, and P. C. Marchisio. 1991. The role of integrins in the maintenance of endothelial monolayer integrity. *J. Cell Biol.* 112:479–490.

10. Moy, A. B., M. Winter, A. Kamath, K. Blackwell, G. Reyes, I. Giaever, C. Keese, and D. M. Shasby. 2000. Histamine alters endothelial barrier function at cell-cell and cell-matrix sites. *Am. J. Physiol. Lung Cell. Mol. Physiol.* 278:L888–L898.

11. Carrillo, A., S. Chamorro, M. Rodriquez-Gago, B. Alvarez, M. J. Molina, J. I. Rodriguez-Barbosa, A. Sanchez, P. Ramirez, A. Munoz, J. Dominguez, P. Parrilla, and J. Yelamos. 2002. Isolation and characterization of immortalized porcine aortic endothelial cell lines. *Vet. Immunol. Immunopathol.* 89:91–98.

12. Schelling, M. E., C. J. Meininger, J. R. Hawker, Jr., and H. J. Granger. 1988. Venular endothelial cells from bovine heart. *Am. J. Physiol.* 254: H1211–H1217.

13. Binnig, G., C. F. Quate, and C. H. Gerber. 1986. Atomic force microscope. *Phys. Rev. Lett.* 56:930–933.

14. Lal, R., and S. A. John. 1994. Biological applications of atomic force microscopy. *Am. J. Physiol.* 266:C1–C21.

15. Radmacher, M., R. W. Tillman, M. Fritz, and H. E. Gaub. 1992. From molecules to cells: imaging soft samples with the atomic force microscope. *Science.* 257:1900–1905.

16. Karrasch, S., R. Hegerl, J. H. Hoh, W. Baumeister, and A. Engel. 1994. Atomic force microscopy produces faithful high-resolution images of protein surfaces in an aqueous environment. *Proc. Natl. Acad. Sci. USA.* 91:836–838.

17. Shroff, S. G., D. R. Saner, and R. Lal. 1995. Dynamic micromechanical properties of cultured rat atrial myocytes measured by atomic force microscopy. *Am. J. Physiol.* 269:C286–C292.

18. Wojcikiewicz, E. P., X. Zhang, and V. T. Moy. 2004. Force compliance measurements on living cells using atomic force microscopy (AFM). *Biol. Proced. Online.* 6:1–9.

19. Willemsen, O. H., M. M. Snel, A. Cambi, J. Greve, B. G. De Grooth, and C. G. Figdor. 2000. Biomolecular interactions measured by atomic force microscopy. *Biophys. J.* 79:3267–3281.

20. Yuan, C., A. Chen, P. Kolb, and V. T. Moy. 2000. Energy landscape of streptavidin-biotin complexes measured by atomic force microscopy. *Biochemistry.* 39:10219–10223.

21. Florin, E., V. T. Moy, and H. E. Gaub. 1994. Adhesion forces between individual ligand-receptor pairs. *Science.* 264:415–417.

22. Moy, V. T., E. Florin, and H. E. Gaub. 1994. Intermolecular forces and energies between ligands and receptors. *Science.* 266:257–259.

23. Hutter, J. L., and J. Bechhoefer. 1993. Calibration of atomic force microscope tips. *Rev. Sci. Instrum.* 64:1868–1873.

24. Walters, D. A., J. P. Cleveland, N. H. Thomson, P. K. Hansma, M. A. Wendman, G. Gurley, and V. Elings. 1996. Short cantilevers for atomic force microscopy. *Rev. Sci. Instrum.* 67:3583–3590.

25. Lehenkari, P. P., and M. A. Horton. 1999. Single integrin adhesion forces in intact cells measured by atomic force microscopy. *Biochem. Biophys. Res. Commun.* 259:645–650.

26. Hinterdorfer, P., F. Kienberger, A. Raab, H. J. Gruber, G. W. Baumgartner, G. Kada, C. Riener, S. Wielert-Badt, C. Borken, and H. Schindler. 2000. Poly(ethylene glycol): an ideal spacer for molecular recognition force microscopy/spectroscopy. *Single Mol.* 1:99–103.

27. Hertz, H. 1881. Ueber die beruhrung fester elastischer korper. *J. Reine. Angew. Math.* 92:156–171.

28. Li, F., S. D. Redick, H. P. Erickson, and V. T. Moy. 2003. Force measurements of the $\alpha 5\beta 1$ integrin-fibronectin interaction. *Biophys. J.* 84:1252–1262.

29. Baumgartner, W., P. Hinterdorfer, and H. Schindler. 2000. Data analysis of interaction forces measured with the atomic force microscope. *Ultramicroscopy.* 82:85–95.

30. Sneddon, I. N. 1965. The relation between load and penetration in the axisymmetric Boussinesq problem for a punch of arbitrary profile. *Int. J. Eng. Sci.* 3:47–57.

31. Vinckier, A., and G. Semenza. 1998. Measuring elasticity of biological materials by atomic force microscopy. *FEBS Lett.* 430:12–16.

32. Weisenhorn, A. L., M. Khorsandi, S. Kasas, V. Gotzos, and H. J. Butt. 1993. Deformation and height anomaly of soft surfaces studied with an AFM. *Nanotechnology.* 4:106–113.

33. You, H. X., and L. Yu. 1999. Atomic force microscopy imaging of living cells: progress, problems and prospects. *Methods Cell Sci.* 21:1–17.

34. Pierschbacher, M. D., and E. Ruoslahti. 1987. Influence of stereochemistry of the sequence Arg-Gly-Asp-Xaa on binding specificity in cell adhesion. *J. Biol. Chem.* 262:17294–17298.

35. Lum, H., and A. B. Malik. 1994. Regulation of vascular endothelial barrier function. *Am. J. Physiol.* 267:L223–L241.

36. Sims, J. R., S. Karp, and D. E. Ingber. 1992. Altering the cellular mechanical force balance results in integrated changes in cell, cytoskeletal and nuclear shape. *J. Cell Sci.* 103:1215–1222.

37. Mathur, A. B., A. M. Collinsworth, W. M. Reichert, W. E. Kraus, and G. A. Truskey. 2001. Endothelial, cardiac muscle and skeletal muscle exhibit different viscous and elastic properties as determined by atomic force microscopy. *J. Biomech.* 34:1545–1553.

38. Radmacher, M. 1997. Measuring the elastic properties of biological samples with the AFM. *IEEE Eng. Med. Biol. Mag.* 16:47–57.

39. Weisenhorn, A. L., P. K. Hansma, T. R. Albrecht, and C. F. Quatel. 1989. Forces in atomic force microscopy in air and water. *Appl. Phys. Lett.* 54:2651–2653.

40. Jiang, G., G. Giannone, D. R. Critchley, E. Fukumoto, and M. Sheetz. 2003. Two-piconewton slip bond between fibronectin and the cytoskeleton depends on talin. *Nature.* 424:334–337.

41. Johansson, S. E. A. 1997. Fibronectin-integrin interactions. *Front. Biosci.* 2:126–146.

42. Chen, A., and V. T. Moy. 2000. Cross-linking of cell surface receptors enhances cooperativity of molecular adhesion. *Biophys. J.* 78:2814–2820.

43. Pierres, A., A. Benoliel, and P. Bongrand. 1998. Studying receptor-mediated cell adhesion at the single molecule level. *Cell Adhes. Commun.* 5:375–395.

44. Merkel, R., P. Nassoy, A. Leung, K. Ritchie, and E. Evans. 1999. Energy landscapes of receptor-ligand bonds explored with dynamic force spectroscopy. *Nature.* 397:50–53.

45. Choquet, D., D. P. Felsenfeld, and M. Sheetz. 1997. Extracellular matrix rigidity causes strengthening of integrin-cytoskeleton linkages. *Cell.* 88:39–48.

46. Cattelino, A., C. Albertinazzi, M. Bossi, D. R. Critchley, and I. de Curtis. 1999. A cell-free system to study regulation of focal adhesions and of the connected actin cytoskeleton. *Mol. Biol. Cell.* 10:373–391.

47. Broday, D. 2000. Diffusion of clusters of transmembrane proteins as a model of focal adhesion remodeling. *Bull. Math. Biol.* 62:891–924.

48. Trepat, X., M. Grabulosa, L. Buscemi, F. Rico, R. Farre, and D. Navajas. 2005. Thrombin and histamine induce stiffening of alveolar epithelial cells. *J. Appl. Physiol.* 98:1567–1574.

49. Hohenester, E., and J. Engel. 2002. Domain structure and organization in extracellular matrix proteins. *Matrix Biol.* 21:115–128.

50. Miyazaki, H., and K. Hayashi. 1999. Atomic force microscopic measurement of the mechanical properties of intact endothelial cells in fresh arteries. *Med. Biol. Eng. Comput.* 37:530–536.

51. Davies, P. F., T. Mundel, and K. A. Barbee. 1995. A mechanism for heterogeneous endothelial responses to flow in vivo and in vitro. *J. Biomech.* 28:1553–1560.